Thermodynamic constraint on the depth of the global tropospheric circulation

David W. J. Thompson[a,1], Sandrine Bony[b], and Ying Li[a]

[a]Department of Atmospheric Science, Colorado State University, Fort Collins, CO 80523; and [b]Sorbonne Université, LMD/IPSL, CNRS, Univ Paris 06, 75252 Paris, France

Edited by Isaac M. Held, Geophysical Fluid Dynamics Laboratory, National Oceanic and Atmospheric Administration, Princeton, NJ, and approved May 24, 2017 (received for review December 14, 2016)

The troposphere is the region of the atmosphere characterized by low static stability, vigorous diabatic mixing, and widespread condensational heating in clouds. Previous research has argued that in the tropics, the upper bound on tropospheric mixing and clouds is constrained by the rapid decrease with height of the saturation water vapor pressure and hence radiative cooling by water vapor in clear-sky regions. Here the authors contend that the same basic physics play a key role in constraining the vertical structure of tropospheric mixing, tropopause temperature, and cloud-top temperature throughout the globe. It is argued that radiative cooling by water vapor plays an important role in governing the depth and amplitude of large-scale dynamics at extratropical latitudes.

climate dynamics | climate change | cloud feedbacks | extratropical dynamics | general circulation

The defining difference between the troposphere (the turning sphere) and the stratosphere (the layered sphere) is the amplitude of mixing within each region. The troposphere is marked by vigorous diabatic motions (i.e., motions that flux heat across isentropic surfaces); the stratosphere is characterized by relatively weak diabatic mixing.

The top of the troposphere coincides closely to the level above which clouds rarely penetrate. In the tropics, the upper bound on tropospheric clouds is believed to be strongly constrained by the unique vertical structure of radiative cooling by water vapor. Saturation vapor pressure decreases rapidly with temperature in the tropical upper troposphere in accordance with the Clausius–Clapeyron relationship. As the saturation vapor pressure decreases, so do water vapor concentrations, and hence so does the amplitude of the clear-sky radiative cooling (1, 2) and its associated downward mass flux (3). From continuity, the thermodynamic limit on sinking motion in clear-sky regions extends to rising motion in regions of deep convection (3). Because the rising motion in regions of deep convection is limited by saturation vapor pressures (and thus temperatures) in clear-sky regions and the static stabilities in clear-sky and cloudy regions of the tropics are comparable, it follows that cloud-top temperatures in the tropics are strongly constrained by the basic thermodynamics that govern clear-sky water vapor concentrations (3, 4).

The physical linkages between clear-sky radiative cooling, the depth of tropospheric mixing, and clouds have been applied specifically to the case of tropical anvil clouds. Here we contend that the same physical linkages play an even broader role in the global atmosphere circulation. It is argued that clear-sky cooling by water vapor constrains the depth of tropospheric mixing, cloud-top temperatures, and the amplitude of large-scale atmospheric dynamics throughout the global atmosphere.

A Thermodynamic Constraint on the Depth of the Troposphere

At steady state, the thermodynamic energy equation can be expressed in pressure coordinates as

$$V \cdot \nabla_h T - \omega S = Q, \qquad [1]$$

Where $V \cdot \nabla_h T$ is the horizontal advection of temperature, ω is the vertical velocity in pressure coordinates, S is the static stability (see *Supporting Information* for definition), and Q denotes heating due to diabatic processes.

The vertical motion term in **[1]** can be divided into two components: (*i*) an adiabatic component that balances the horizontal temperature advection and (*ii*) a "residual" component that balances diabatic heating. Hence,

$$\omega_A \equiv \frac{V \cdot \nabla_h T}{S} \qquad [2]$$

is the adiabatic vertical motion required to balance temperature advection by the horizontal flow and

$$\omega_D \equiv \omega - \omega_A = -\frac{Q}{S} \qquad [3]$$

is the cross-isentropic vertical motion required to balance diabatic heating. The zonal average of ω_D is analogous to the residual circulation in the transformed Eulerian mean (TEM) (e.g., ref. 5).

In the Tropics. At tropical latitudes, horizontal temperature advection is very small, and thus $|\omega_A| \sim 0$ and the dominant balance in the thermodynamic energy equation is between diabatic vertical motion and heating ($\omega \sim \omega_D = -\frac{Q}{S}$). In regions of rising air, the diabatic motion is balanced predominantly by condensational heating; in regions of sinking air, it is balanced mainly by the emission of thermal infrared radiation to space by water vapor.

Significance

The study explores two fundamental problems in climate science: (*i*) The physical factors that govern the depth of the troposphere, and (*ii*) the response of clouds to climate change. Previous research has argued that tropical anvil temperatures are strongly constrained by the fundamental thermodynamic properties of water vapor. Here we argue that the same basic thermodynamic properties strongly constrain the depth of the troposphere, the temperature of high clouds, and the amplitude of large-scale dynamics throughout the globe. The results suggest that the positive climate feedbacks associated with tropical high clouds also operate in the extratropics, and that the top of the troposphere should remain at roughly the same temperature throughout the globe as the climate system warms.

Author contributions: D.W.J.T., S.B., and Y.L. designed research, performed research, analyzed data, and wrote the paper.

The authors declare no conflict of interest.

This article is a PNAS Direct Submission.

Freely available online through the PNAS open access option.

[1]To whom correspondence should be addressed. Email: davet@atmos.colostate.edu.

This article contains supporting information online at www.pnas.org/lookup/suppl/doi:10.1073/pnas.1620493114/-/DCSupplemental.

As noted in the Introduction, the balance between sinking diabatic motion and radiative cooling by water vapor has important implications for anvil cloud temperature and amount in the upper tropical troposphere (3, 4, 6).

In the Extratropics. At first glance, the linkages between water vapor radiative cooling, cloud-top temperature, and cloud fraction do not appear to hold in the extratropics, where the horizontal temperature gradients are large and thus (*i*) vertical motion is balanced by both horizontal temperature advection and diabatic heating, and (*ii*) the static stabilities in clear-sky and cloudy regions are not constrained to be similar. However, temperature advection can only redistribute thermal energy and—over a suitably large vertical and horizontal domain—does not balance diabatic heating. Furthermore, the static stabilities averaged over clear-sky and cloudy regions of the extratropics are not markedly different, at least in the long-term zonal mean (Fig. S1). As such, even in the extratropics, the net rising motion associated with diabatic heating in cloudy regions must be balanced by sinking motion associated with radiative cooling due to water vapor in clear-sky regions. That is, the linkages between water vapor radiative cooling, cloud temperature, and anvil-cloud height found in the tropics should also hold at extratropical latitudes.

To the extent that Q in clear-sky regions is dominated by water vapor radiative cooling, it follows that the balance in Eq. **3** has important implications for the structure of the troposphere not only at tropical latitudes, but at extratropical latitudes as well. We hypothesize that the distinctive vertical structure of clear-sky radiative cooling by water vapor provides a key constraint on the depth of diabatic mixing and thus on the depth of the troposphere throughout the globe.

Supporting Evidence

The hypothesis is tested in observations of: (*i*) Cloud incidence and clear-sky radiative cooling rates derived from *CloudSat* and *CALIPSO* (Cloud-Aerosol Lidar and Infrared Pathfinder Satellite Observations) satellite data (7–9). Cloud incidence is calculated following the methodology in ref. 10; (*ii*) temperature and static stability derived from the *CloudSat*/European Centre for Medium-Range Weather Forecasts auxiliary product (ECMWF-AUX), which provides ECMWF state variable data at the space/time resolution of the *CloudSat* satellite track; (*iii*) water vapor volume mixing ratio from the Microwave Limb Sounder (MLS)/Aura data (https://mls.jpl.nasa.gov/products/h2o_product.php); and (*iv*) eddy fluxes of potential vorticity from the ECMWF Interim Reanalysis [ERA-Interim (11)].

Because *CloudSat* has limited spatial and temporal sampling, all results are also calculated for climate output from a general circulation model with explicit shortwave and longwave radiation schemes [the Institut Pierre Simon Laplace general circulation model version CM5A-LR (IPSL-CM5A-LR) (12, 13)]. We use two numerical simulations: (*i*) a simulation forced with observed time-varying sea surface temperatures from 1979 to 2008 [e.g., the Atmospheric Model Intercomparison Project (AMIP) configuration used in the Coupled Model Intercomparison Project phase 5 (CMIP5)]; (*ii*) a simulation forced with sea surface temperatures raised by 4 K relative to their 1979–2008 values (e.g., the AMIP+4K configuration used in CMIP5). Results from the run forced with observed sea surface temperatures are shown in Figs. 1–6; results from the AMIP+4K run are shown in Fig. 5. Additional details of the data, model output, and diagnostic techniques are provided in the *Supporting Information*.

Fig. 1, *Top,* shows the clear-sky radiative heating rates (Q_r; contours) and associated clear-sky diabatic vertical mass fluxes ($-\frac{Q_r}{S}$; shading) from *CloudSat* observations (Fig. 1, *Left*) and output from the IPSL simulation forced with observed sea surface temperatures (Fig. 1, *Right*). The clear-sky heating rates and vertical mass fluxes peak in the tropical troposphere and decrease with both latitude and altitude, such that isopleths of constant heating rates and mass fluxes generally slope downward with latitude from the tropics to the poles. The clear-sky vertical mass fluxes mainly mirror the clear-sky radiative cooling rates, except in the

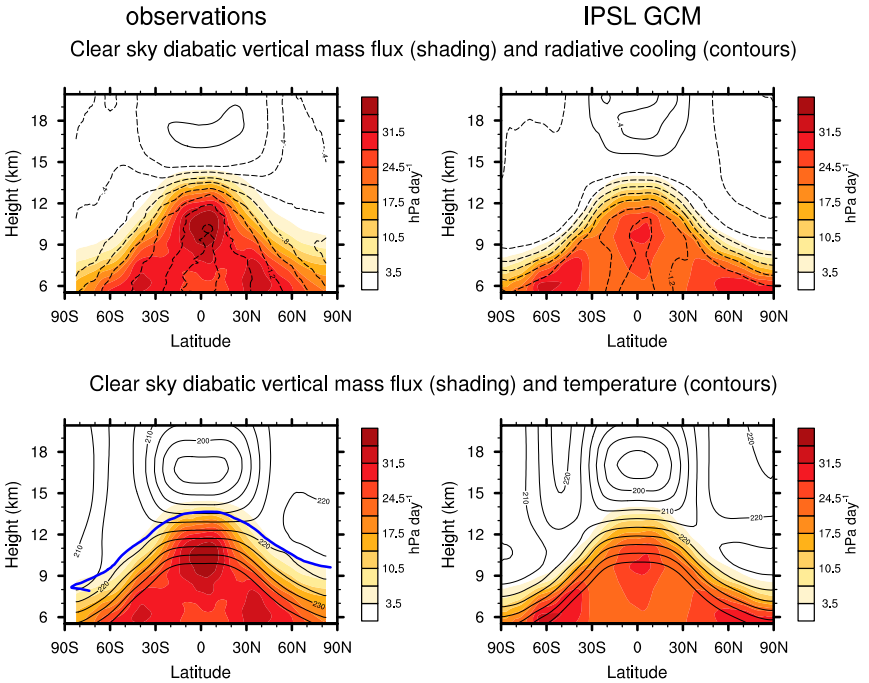

Fig. 1. (*Top*) Clear-sky radiative cooling (contours) overlaid with the diabatic vertical mass flux calculated as −Qr/S (shading). (*Bottom*) Clear-sky diabatic vertical mass flux (shading) superposed on temperature (contours). The thick blue line in *Bottom Left* indicates the 20 ppmv isopleth based on the MLS water vapor data. Results in the *Left* are derived from observations. Results in the *Right* are derived from the IPSL general circulation model (GCM). Observations are based on *CloudSat* clear-sky cooling rates and the *CloudSat* ECWMF-AUX product.

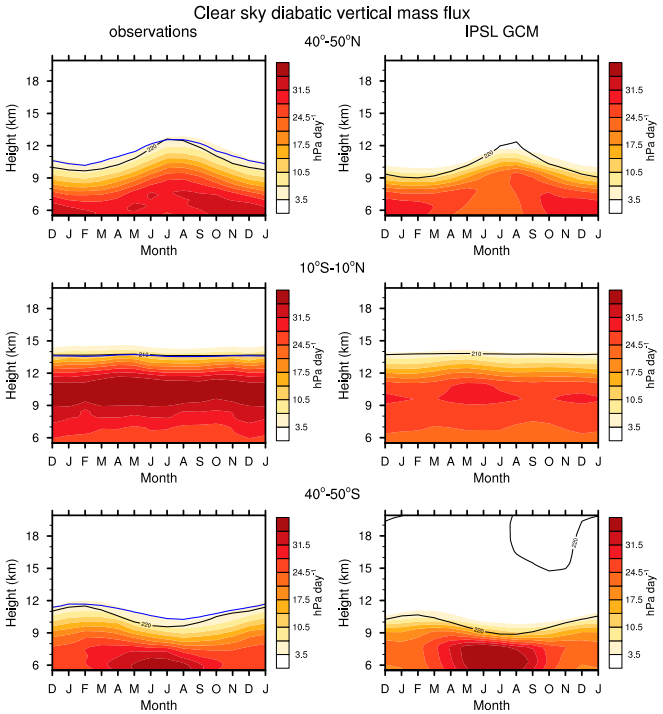

Fig. 2. Clear-sky diabatic vertical mass flux (shading) for indicated latitude bands as a function of calendar month and altitude. The black lines indicate the 220K isotherm (*Top* and *Bottom*) and 210K isotherm (*Middle*). The blue lines on all panels indicate the 20 ppmv water vapor isopleth. Results in the *Left* are derived from observations. Results in the *Right* are derived from the IPSL general circulation model (GCM).

free troposphere <~9 km in the tropics and <~6 km in the extratropics, where regions of relatively low static stability (e.g., ref. 14) are associated with regions of relatively high mass fluxes.

For the most part, the observed clear-sky radiative heating rates and vertical mass fluxes are noisier and larger than their climate simulation counterparts. The differences between the observed and simulated results may arise from a variety of factors including, for example, the effects of orbital and clear-sky sampling on the observations, the limitations of the general circulation model, and the limitations of the *CloudSat* flux algorithm. What is important is that the global-scale features in the clear-sky mass fluxes are qualitatively similar in both the observations and climate model output.

The most prominent features in the clear-sky diabatic vertical mass fluxes are the negative vertical gradients found between 7 and 9 km at middle latitudes and 12 and 14 km in the tropics. The vertical gradients in the annual-mean mass fluxes are larger in the tropics than in the extratropics. However, the differences in amplitudes between the vertical gradients in tropical and extratropical mass fluxes are in part an artifact of the annual averaging: The largest gradients in the mass fluxes occur at roughly the same altitude throughout the year in the tropics, whereas they rise and fall with the seasonal cycle in the extratropics and are thus smeared out in the annual mean there (Fig. 2).

As reviewed earlier, the large vertical gradients in the clear-sky mass fluxes in the upper troposphere arise in part from the temperature dependence of the water vapor mixing ratio (1, 2). The clear-sky mass fluxes become very small (e.g., drop below ~5 hPa/day) at comparably low water vapor concentrations (volume mixing ratios of roughly 20 ppmv) at both tropical and extratropical latitudes (Fig. 1, *Bottom Left*) and throughout the calendar year (Fig. 2, *Left*), which hints at the importance of water vapor cooling for constraining the clear-sky diabatic vertical motion across the globe. Interestingly, the clear-sky mass fluxes drop below ~5 hPa/day at roughly the same water vapor volume mixing ratio (and likewise, specific humidity) at tropical and extratropical latitudes, but at notably different temperatures: ~210 K in the tropics but ~220 K in the extratropics (Fig. 1, *Bottom*; Fig. 2).

Why does the top of the tropospheric mixing layer (i.e., the level where the clear-sky mass fluxes decrease rapidly with height) occur at different temperatures in the tropics and extratropics? Relative to the tropical upper troposphere, the extratropical upper troposphere is marked by comparatively high static stabilities (*Supporting Information*; ref. 14) and low relative humidities (15), in part due to the efficiency of extratropical eddies in entraining stable, dry air from the extratropical lower stratosphere. Both factors should contribute to relatively warm conditions at the top of the tropospheric mixing layer at extratropical latitudes: (*i*) the clear-sky sinking motion required to balance water vapor cooling is smaller—and thus the level of rapidly decreasing mass fluxes is shifted downward to warmer temperatures—in regions of comparatively high static stability (4, 16, 17). (*ii*) It is the concentration of water vapor (and thus the specific humidity) that matters most for water vapor cooling. Because the relative humidity of the extratropical upper troposphere is relatively low, water vapor concentrations at the 220 K isotherm are somewhat lower in the extratropics than they are in the tropics (Figs. 1, *Bottom*, and 2).

How do the clear-sky diabatic vertical mass fluxes relate to the depth of the troposphere? The depth of the troposphere—and thus the height of the tropopause—can be defined in a variety of ways, all of which give slightly different results (e.g., see discussions in refs. 18–20). Lapse-rate definitions are widely used and simple to calculate, but are not necessarily physically meaningful; potential vorticity definitions are dynamically meaningful at extratropical latitudes, but not at the equator. One simple definition

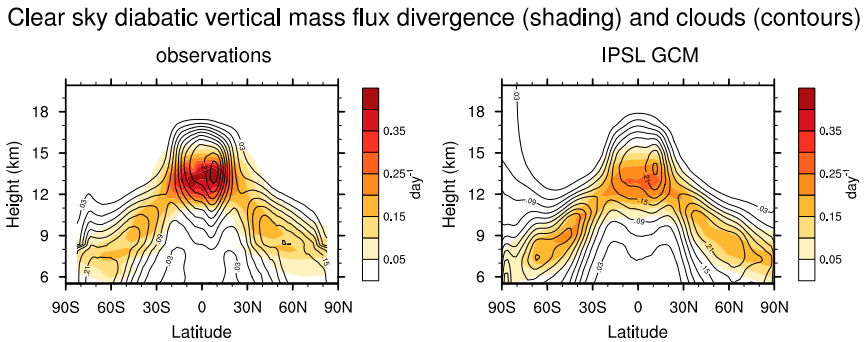

Fig. 3. Clear-sky diabatic vertical mass flux divergence (shading) superposed on cloud incidence (contours). Results in the *Left* are derived from observations. Results in the *Right* are derived from the IPSL general circulation model (GCM). Cloud incidence is derived from *CloudSAT*.

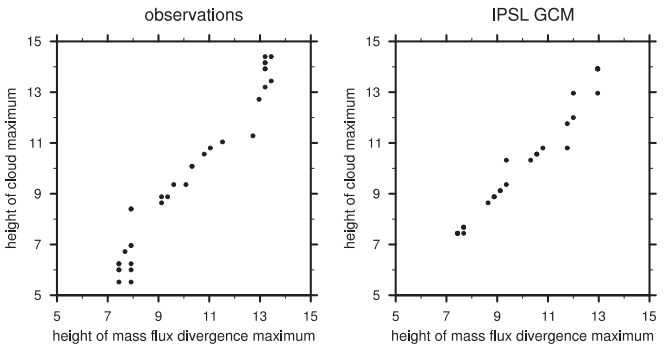

Fig. 4. Scatter plots of the altitudes of maximum clear-sky diabatic vertical mass flux divergence and maximum cloud incidence. Each dot represents a different latitude band. Results in the *Left* are derived from observations. Results in the *Right* are derived from the IPSL general circulation model (GCM).

is the top of the well-mixed layer where convection and radiation are the dominant terms in the thermodynamic energy equation. As such, the top of the majority of latent heating—and thus cloud incidence—can be viewed as a proxy for the depth of the troposphere.

Fig. 3 shows annual-mean cloud incidence superposed on the clear-sky vertical mass flux divergence (i.e., $\frac{\partial}{\partial p}\left(-\frac{Q_r}{S}\right)$). Fig. 4 shows the scatter plot of the altitudes of maximum clear-sky vertical mass flux divergence (abscissa) and maximum cloud incidence (ordinate) as a function of latitude. (Note that positive values of the clear-sky vertical mass flux divergence indicate regions where the clear-sky downward mass fluxes decrease rapidly with height, and thus where the horizontal mass fluxes are converging in clear-sky regions and diverging in cloudy regions). The largest vertical mass flux divergences clearly coincide with the region of largest cloud incidences at all latitudes. The close correspondences highlighted in Fig. 3 are important, because they imply that the static stability in the clear and cloudy regions of the extratropics are sufficiently similar to link the diabatic vertical mass fluxes (Eq. **3**) in both regions. The strong collocation shown in Fig. 3 highlights a key aspect of the extratropical circulation that has not been appreciated in previous work: Cloud-top height—and thus the depth of the troposphere—is coincident with the large vertical gradients in the clear-sky diabatic mass flux not only in the tropics, but in the extratropics as well.

If clear-sky cooling by water vapor constrains cloud fraction throughout the globe, then the temperature of the maximum in cloud fraction should be largely decoupled from surface temperature at all latitudes. The black lines in Fig. 5 show the pressure (*Left*) and temperature (*Right*) of the maximum in cloud fraction as a function of latitude for the same climate model output shown in Fig. 3, *Right*. The red lines show the pressure and temperature of the maximum in cloud fraction when surface temperatures are increased uniformly by 4 K (see *Supporting Information* for simulation details). As expected from ref. 3, the cloud fraction maximum moves to notably lower pressure but stays at roughly the same temperature in the tropics. As demonstrated in Fig. 5, the same basic physical responses are found at extratropical latitudes as well. (The small increases in cloud temperatures in the tropics are consistent with the attendant changes in tropospheric static stability, which act to move the level of largest clear-sky vertical mass fluxes to a slightly warmer level; ref. 4).

Implications for Large-Scale Extratropical Dynamics

The thermodynamic constraints placed on clear-sky radiative cooling also have potential implications for large-scale extratropical dynamics. The steady-state, zonally averaged zonal momentum and thermodynamic energy equations can be expressed as:

$$f\bar{v}^* = -\overline{v'q'} \quad [4]$$

$$\bar{\omega}^* = -\frac{\bar{Q}}{S}, \quad [5]$$

where overbars denote zonal averages, primes denote departures from the zonal average, $\bar{\omega}^* \equiv \bar{\omega} + \frac{\partial}{\partial y}\frac{\overline{v'\theta'}}{S}$ is the TEM vertical wind, $\bar{v}^*$ the TEM meridional wind, and q is the quasigeostrophic (QG) potential vorticity (PV). In the QG approximation, the meridional fluxes of potential vorticity are equivalent to the divergence of the Eliassen–Palm (EP) flux (southward PV fluxes correspond to regions of EP-flux convergence and thus wave breaking). The residual vertical velocity $\bar{\omega}^*$ is expressed in pressure coordinates and is the zonal-mean analog of ω_D in Eq. **3**.

By construction, the TEM vertical motion $\bar{\omega}^*$ is the component of the zonal-mean vertical velocity that is balanced entirely by diabatic processes and thus approximates the zonal-mean diabatic vertical mass flux. In the long-term mean, $\bar{\omega}^*$ is downward over the high latitudes of both hemispheres (e.g., ref. 21). At tropospheric levels, the downward motion in $\bar{\omega}^*$ at high latitudes is balanced primarily by radiative cooling by water vapor, and is thus subject to the same thermodynamic constraints that limit the clear-sky mass flux.

The TEM vertical motion is connected to the TEM meridional motion through continuity. Taking the meridional derivative of Eq. **4**, the vertical derivative of Eq. **5**, and combining through the mass-continuity equation yields:

$$-\frac{\partial}{\partial y}\frac{\overline{v'q'}}{f} = \frac{\partial}{\partial p}\frac{\bar{Q}}{S}. \quad [6]$$

Eq. **6** states that the divergence of the meridional PV flux is balanced by the divergence of the diabatic vertical mass flux. If the meridional scale of the wave motions is comparable at all levels, then the divergence of the meridional PV flux will have largest amplitude at the same altitude that the PV flux does. Thus, the level of largest PV fluxes should coincide with the level of largest diabatic vertical mass flux divergence, i.e., the top of the layer in which infrared cooling by water vapor is important. As shown in Fig. 6, there is, in fact, strong correspondence between the clear-sky diabatic vertical mass flux divergence and wave breaking throughout the extratropics. Some level of agreement between the divergence of the clear-sky vertical mass fluxes

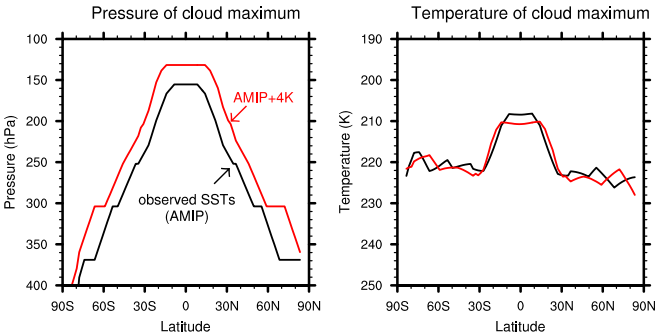

Fig. 5. The pressure (*Left*) and temperature (*Right*) of the maximum in cloud fraction as a function of latitude for climate model output from the IPSL general circulation model (GCM). The black lines indicate results from a simulation forced with time-varying sea surface temperatures (SST) from 1979 to 2008 (observed SSTs; AMIP). The red lines indicate results from a simulation where sea surface temperatures are increased everywhere by 4 K relative to their 1979–2008 values (AMIP+4K). Results are smoothed with a latitudinal running mean filter for display purposes only.

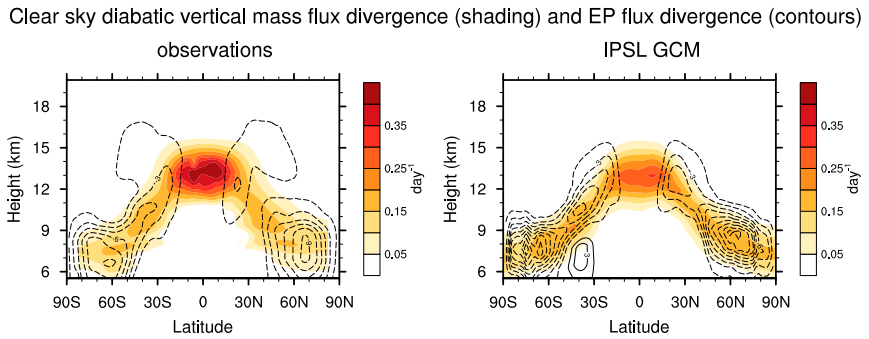

Fig. 6. Clear-sky diabatic vertical mass flux divergence (shading) superposed on the EP flux divergence (contours). Results in the *Left* are derived from observations. Results in the *Right* are derived from the IPSL general circulation model (GCM).

and the PV fluxes is expected from mass continuity. However, the agreement also suggests that the vertical profile of water vapor radiative cooling provides a strong constraint on the vertically varying amplitude of extratropical wave driving. The results suggest that the depth of slantwise convection associated with baroclinic instability in the extratropics and deep convection in the tropics are both constrained by the same basic physics.

Concluding Remarks

The depth of the troposphere is strongly influenced by a range of physical factors, including, for example, surface temperature and tropospheric convection (e.g., refs. 1, 18, 22–24), large-scale extratropical dynamics (e.g., refs. 22, 25–31), and stratospheric dynamics (e.g., refs. 19, 32–35). It is frequently viewed in the context of a radiative constraint and a dynamic constraint (22, 23, 30). The former constraint limits the depth of tropospheric mixing to levels where the radiative equilibrium profile must be convectively adjusted to remain statically stable. The latter constraint accounts for the horizontal fluxes of heat and their influence on the temperature profile at tropospheric levels.

The findings presented here suggest that the Clausius–Clapeyron relationship provides an additional thermodynamic constraint on the depth of the troposphere not only in the tropics, but throughout the global atmosphere. That is, they suggest that the radiative constraint is limited by both the dependence of longwave radiation on moisture, and the dependence of moisture on temperature. The thermodynamic constraint arises from the large vertical gradients in the emission and absorption of longwave radiation by water vapor at upper tropospheric levels which, in turn, arise from the temperature dependence of saturation vapor pressure. As temperature drops with height in the upper troposphere, so do water vapor concentrations in accordance with the Clausius–Clapeyron relation, and hence so does the radiative cooling by water vapor. Altitudes at which temperatures are warm enough to support large water vapor concentrations are characterized by robust clear-sky cooling by water vapor and are thus conducive to vigorous diabatic mixing; altitudes above this level support only weak clear-sky cooling and thus relatively modest diabatic mixing.

As evidence, we have demonstrated that the meridionally and vertically varying structures of the clear-sky diabatic vertical mass fluxes (*i*) vanish at roughly the same water vapor concentrations at all latitudes and (*ii*) closely match the structures of cloud incidence and atmospheric wave driving across much of the globe. The former suggests that the rapid decreases in clear-sky diabatic vertical mass fluxes at the tropopause level arise from the similarly rapid decreases in water vapor concentrations and thus radiative cooling by water vapor. The latter suggests that clear-sky cooling by water vapor strongly constrains the depth of diabatic mixing not only by convection (3), but also by large-scale extratropical eddies. We have also demonstrated that the cloud fraction maximum moves to notably lower pressure but stays at roughly the same temperature throughout the globe in numerical experiments where sea surface temperatures are increased uniformly by 4 K.

The physics exploited in this study apply to any atmosphere that selectively absorbs radiation at terrestrial wavelengths. Pure radiative equilibrium in such an atmosphere yields a temperature profile that transitions smoothly from a statically unstable lower layer to a stable upper layer (1). Because the lower layer is statically unstable, it must be well mixed by convection and a discontinuity—i.e., a tropopause—will form between a well-mixed lower layer that is in radiative–convective equilibrium and a stable upper layer that is in pure radiative equilibrium (1). The results shown here do not suggest that water vapor "causes" a tropopause to form in Earth's atmosphere. Rather, they suggest that water vapor provides a key constraint on the temperature at the top of the tropospheric mixing layer across the globe.

The hypothesis outlined here has several implications for climate variability and change:

i) It provides a physical basis for interpreting the result that the positive feedbacks due to rising high clouds under climate change are not limited to the tropics, but also extend to extratropical latitudes (36, 37). The potential for cloud feedbacks at extratropical latitudes due to the static stability/iris mechanism (6) could be explored in future research.

ii) It predicts that the temperature of the tropopause should remain largely invariant as the troposphere warms, and thus provides a physical basis for interpreting the lifting of the tropopause and deepening of the troposphere under climate change (e.g., refs. 38–40).

iii) It suggests that mixing by baroclinic instability and thus extratropical wave driving is strongly constrained by the vertical gradients in water vapor radiative cooling rates.

iv) It suggests that the level of largest clear-sky diabatic vertical mass flux divergence provides a simple, robust and physically meaningful definition for the depth of the tropospheric mixing layer at both tropical and extratropical latitudes.

ACKNOWLEDGMENTS. We thank John M. Wallace, Kerry A. Emanuel, Brian J. Hoskins, Dennis L. Hartmann, Mark D. Zelinka, Thomas Birner, two anonymous reviewers, and the PNAS editor for insightful and helpful comments on the manuscript. We also thank Mijeong Park for providing monthly mean versions of the MLS data. D.W.J.T. is funded by the National Science Foundation (NSF) Climate Dynamics Program. S.B. is supported by the European Research Council (ERC Grant 694768). Y.L. is funded by *CloudSAT* via National Aeronautics and Space Administration Jet Propulsion Laboratory and the NSF Climate Dynamics Program.

1. Manabe S, Strickler RF (1964) Thermal equilibrium of the atmosphere with a convective adjustment. *J Atmos Sci* 21:361–385.
2. Hartmann DL, Holton JR, Fu Q (2001) The heat balance of the tropical tropopause, cirrus and stratospheric dehydration. *Geophys Res Lett* 28:1969–1972.
3. Hartmann DL, Larson K (2002) An important constraint on tropical cloud-climate feedback. *Geophys Res Lett* 29:1951–1954.
4. Zelinka MD, Hartmann DL (2010) Why is longwave cloud feedback positive? *J Geophys Res* 115:D16117.
5. Andrews DG, McIntyre ME (1976) Planetary waves in horizontal and vertical shear: The generalized Eliassen–Palm relation and the mean zonal acceleration. *J Atmos Sci* 33:2031–2048.
6. Bony S, et al. (2016) Thermodynamic control of anvil cloud amount. *Proc Natl Acad Sci USA* 113:8927–8932.
7. Mace GG, et al. (2009) A description of hydrometeor layer occurrence statistics derived from the first year of merged CloudSat and CALIPSO data. *J Geophys Res* 114: D00A26.
8. Henderson DS, L'Ecuyer T, Stephens G, Partain P, Sekiguchi M (2013) A multisensor perspective on the radiative impacts of clouds and aerosols. *J Appl Meteorol Climatol* 52:853–871.
9. Haynes JM, Haar THV, L'Ecuyer T, Henderson D (2013) Radiative heating characteristics of Earth's cloudy atmosphere from vertically resolved active sensors. *Geophys Res Lett* 40:624–630.
10. Li Y, Thompson DWJ, Stephens GL, Bony S (2014) A global survey of the instantaneous linkages between cloud vertical structure and large-scale climate. *J Geophys Res Atmos* 119:3770–3792.
11. Dee DP, et al. (2011) The ERA-Interim reanalysis: Configuration and performance of the data assimilation system. *Q J R Meteorol Soc* 137:553–597.
12. Dufresne J-L, et al. (2013) Climate change projections using the IPSL-CM5 Earth system model: From CMIP3 to CMIP5. *Clim Dyn* 40:2123–2165.
13. Hourdin F, et al. (2006) The LMDZ4 general circulation model: Climate performance and sensitivity to parameterized physics with emphasis on tropical convection. *Clim Dyn* 27:787–813.
14. Grise KM, Thompson DWJ, Birner T (2010) A global survey of static stability in the stratosphere and upper troposphere. *J Clim* 23:2275–2292.
15. Gettelman A, et al. (2006) Climatology of upper-tropospheric relative humidity from the atmospheric infrared sounder and implications for climate. *J Clim* 19:6104–6121.
16. Kuang Z, Hartmann DL (2007) Testing the FAT hypothesis in a cloud-resolving model. *J Clim* 20:2051–2057.
17. Harrop BE, Hartmann DL (2012) Testing the role of radiation in determining tropical cloud top temperature. *J Clim* 25:5731–5747.
18. Highwood EJ, Hoskins BJ (1998) The tropical tropopause. *Q J R Meteorol Soc* 124: 1579–1604.
19. Birner T (2010) Residual circulation and tropopause structure. *J Atmos Sci* 67: 2582–2600.
20. Fueglistaler S, et al. (2009) Tropical tropopause layer. *Rev Geophys* 47:RG1004.
21. Edmon HJ, Hoskins BJ, McIntyre ME (1980) Eliassen-Palm cross sections for the troposphere. *J Atmos Sci* 37:2600–2616.
22. Held IM (1982) On the height of the tropopause and the static stability of the troposphere. *J Atmos Sci* 39:412–417.
23. Thuburn J, Craig GC (1997) GCM tests of theories for the height of the tropopause. *J Atmos Sci* 54:869–882.
24. Schneider T (2007) The thermal stratification of the extratropical troposphere. *The Global Circulation of the Atmosphere*, eds Schneider T, Sobel AH (Princeton Univ Press, Princeton, NJ), pp 47–77.
25. Ambaum M (1997) Isentropic formation of the tropopause. *J Atmos Sci* 54:555–568.
26. Haynes P, Scinocca J, Greenslade M (2001) Formation and maintenance of the extratropical tropopause by baroclinic eddies. *Geophys Res Lett* 28:4179–4182.
27. Schneider T (2004) The tropopause and the thermal stratification in the extratropics of a dry atmosphere. *J Atmos Sci* 61:1317–1340.
28. Wirth V, Szabo T (2007) Sharpness of the extratropical tropopause in baroclinic life cycle experiments. *Geophys Res Lett* 34:L02809.
29. Dell'Aquila A, Ruti PM, Sutera A (2007) Effects of the baroclinic adjustment on the tropopause in the NCEP–NCAR reanalysis. *Clim Dyn* 28:325–332.
30. Zurita-Gotor P, Vallis GK (2011) Dynamics of midlatitude tropopause height in an idealized model. *J Atmos Sci* 68:823–838.
31. Wu Y, Pauluis O (2014) Midlatitude tropopause and low-level moisture. *J Atmos Sci* 71:1187–1200.
32. Thuburn J, Craig GC (2000) Stratospheric influence on tropopause height: The radiative constraint. *J Atmos Sci* 57:17–28.
33. Son SW, Lee S, Feldstein SB (2007) Intraseasonal variability of the zonal-mean extratropical tropopause height. *J Atmos Sci* 64:608–620.
34. Haqq-Misra J, Lee S, Frierson DMW (2011) Tropopause structure and the role of eddies. *J Atmos Sci* 68:2930–2944.
35. Barroso JÁ, Zurita-Gotor P (2016) Intraseasonal variability of the zonal-mean extratropical tropopause: The role of changes in polar vortex strength and upper-troposphere wave breaking. *J Atmos Sci* 73:1383–1399.
36. Zelinka MD, Zhou C, Klein SA (2016) Insights from a refined decomposition of cloud feedbacks. *Geophys Res Lett* 43: 10.1002/2016GL069917.
37. Zelinka MD, Klein SA, Hartmann DL (2012) Computing and partitioning cloud feedbacks using cloud property histograms. Part II: Attribution to changes in cloud amount, altitude, and optical depth. *J Clim* 25:3736–3754.
38. Santer BD, et al. (2003) Contributions of anthropogenic and natural forcing to recent tropopause height changes. *Science* 301:479–483.
39. Singh MS, O'Gorman PA (2012) Upward shift of the atmospheric general circulation under global warming: Theory and simulations. *J Clim* 25:8259–8276.
40. Vallis GK, Zurita-Gotor P, Cairns C, Kidston J (2014) Response of the large-scale structure of the atmosphere to global warming. *Q J R Meteorol Soc* 141:1479–1501.